



Synthesis, structural and magnetic properties of $\text{NiFe}_{2-x}\text{La}_x\text{O}_4$ ($0 \leq x \leq 0.10$) nanoparticles

Suman Sharma¹ · Narayan Dutt Sharma¹ · Nisha Choudhary¹ · Mukesh Kumar Verma¹ · Devinder Singh¹

Received: 17 November 2020 / Revised: 14 February 2021 / Accepted: 17 March 2021 / Published online: 24 March 2021
© Australian Ceramic Society 2021

Abstract

Lanthanum substituted nickel ferrites $\text{NiFe}_{2-x}\text{La}_x\text{O}_4$ ($0 \leq x \leq 0.10$) powders have been synthesized for the first time by combustion technique using glycine as a fuel. All the ferrites crystallize in $Fd\bar{3}m$ space group with cubic symmetry. Very small peaks of both Fe_2O_3 and LaFeO_3 were also detected, the intensity of which increases with increasing La content. No systematic trend in the lattice parameter a with La doping has been noticed. Room temperature magnetization studies, obtained from vibrating sample magnetometer (VSM), exhibit a decrease in saturation magnetization with La doping. Cation distribution, obtained from magnetic measurements, shows that La doped nickel ferrites have inverse spinel structure in which Ni^{2+} ions predominantly occupy octahedral sites.

Keywords Combustion technique · XRD · EDX · TEM · Magnetic properties

Introduction

Magnetic spinel ferrites, MFe_2O_4 ($\text{M} = \text{Co}^{2+}, \text{Cu}^{2+}, \text{Ni}^{2+}$, etc.), are significant magnetic materials with several modern technological applications. Their unique properties are governed by their reduced size [1–5]. NiFe_2O_4 have inverse spinel structure in which half of the Fe^{3+} ions reside at A sites and the other half on B sites while other half of the B sites are occupied by Ni^{2+} ions. Therefore, its chemical formula can be written as $(\text{Fe}^{3+})_A [\text{Ni}^{2+}\text{Fe}^{3+}]_B \text{O}_4^{2-}$ [6]. Partial exchange of Fe^{3+} by rare-earth (R^{3+}) ion in the B-site leads to distortion of structure [7] that causes strains and significantly alters the magnetic properties [8–11]. NiFe_2O_4 can be used as a permanent magnet because of its high coercivity. It is very fascinating to examine the introduction of the rare earth ions into the spinel NiFe_2O_4 because their introduction may increase coercivity and hence fabrication of magnetically extra hard materials. Rare earth metal ions, because of their larger sizes, favor holding the octahedral sites. The doping of rare earth metal ions into the structure hinders the growth of the ferrite because

these particles are difficult to diffuse [12, 13]. Ferromagnetism is displayed by nickel ferrites that arise due to the magnetic moment of anti-parallel spins between Ni^{2+} ions residing at octahedral sites and Fe^{3+} ions at tetrahedral sites [14]. Due to partial replacement of Fe ions with rare earth metal ions in the spinel structure, there is introduction of R–Fe and R–R interactions (3d–4f and 4f–4f couplings) in these ferrites and as these interconnections are very low in comparison to Fe–Fe interconnections (3d–3d couplings) and they are the source of reduction in the spontaneous magnetization and Curie temperature values of the rare earth substituted spinel ferrites [13, 15–17].

It is usually known that nanoparticles accompanied by controlled size and composition have many technological advantages. The properties like appearance and dimension of the particles and various physical properties of ferrites are determined by preparation method. The ferrites having large and non-uniform particle size are generated by ceramic technique comprising high-temperature solid-state reactions resulting in the creation of empty space or low density [18]. In recent years, various innovative techniques of synthesis of nanocrystalline ferrites such as co-precipitation, sol-gel, hydrothermal, freeze drying, oxidation, and reverse micelle method have been recommended [19–26]. Among the modern techniques of preparation, combustion technique is proving to be one of the most attractive and effective methods for the synthesis of nanoscale materials as it controls crystallite size, purity, etc.

✉ Devinder Singh
drdssambyal@rediffmail.com

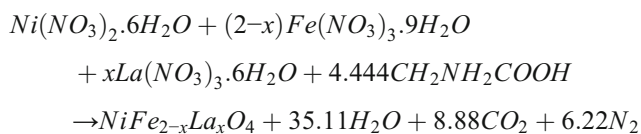
¹ Department of Chemistry, University of Jammu, Jammu 180 006, India

and has been applied for the large-scale generation of nanoparticles with large surface area. It is convenient to check the stoichiometry and surface area that have a great impact on structure, morphology, and magnetic characteristics of ferrites [27]. Various characteristics of this method of synthesis like lesser time, simplicity, less use of energy during preparation are advantageous [28–30].

In the present research, we describe the preparation of nanocrystalline NiFe_2O_4 by simple, fast, and inexpensive combustion method taking glycine as fuel and study the influence of lanthanum substitution for iron on the structural and magnetic properties of nickel ferrite. As far as we know, there is only one report on this aspect [31]. Moreover, there are some contradictory statements about the cell parameters on La-substituted nickel ferrites. Al Angari [31] shows systematic increase in lattice constant a for doping of La in NiFe_2O_4 , while Lin *et al.* [32] reported decrease in lattice constant a for the incorporation of La in $\text{Cu}_{0.5}\text{Co}_{0.5}\text{Fe}_2\text{O}_4$ nanoparticles due to increase in LaFeO_3 impurity. In order to overcome such anomalies, we have carried out Rietveld refinements of XRD patterns.

Experimental

In the present work, $\text{NiFe}_{2-x}\text{La}_x\text{O}_4$ powders were prepared via glycine-nitrate combustion method. The stoichiometric quantities of $\text{Ni}(\text{NO}_3)_2 \cdot 6\text{H}_2\text{O}$, $\text{Fe}(\text{NO}_3)_3 \cdot 9\text{H}_2\text{O}$, $\text{La}(\text{NO}_3)_3 \cdot 6\text{H}_2\text{O}$, and $\text{NH}_2\text{CH}_2\text{COOH}$ (all were 99.9% pure) were dissolved in distilled water, and the volume of the mixture was raised to 200 mL. The pH of the resulting solutions was found to be in the range 1.5–1.8. On the basis of the total oxidizing and reducing valencies of oxidizer and fuel, the stoichiometric ratio of the above mixture was calculated for the combustion technique [33]. The glycine-nitrate ratio has been estimated based on propellant chemistry and the details are reported elsewhere [34]. The resulting mixtures were stirred for about 1 h using a magnetic stirrer followed by heat treatment at 100°C on a hot plate till a viscous gel formation. The gel was then decayed in a preheated oven at 150°C resulting in a frothy residue which was then crushed into powder and heated at 800°C for 10 h in a furnace to disintegrate the organic precursor. The feasible chemical reaction for the preparation of Ni ferrites is given by the following chemical equation:



For the interpretation of crystal structure of synthesized compounds, X-ray diffraction (XRD) analysis of powdered samples has been done using $\text{CuK}\alpha$ ($\lambda = 1.54\text{\AA}$) radiation at room temperature with 2θ altered in the range of $10\text{--}100^\circ$. Rietveld method was employed to get structural parameters by means of the *GSAS* program. Scherrer equation was used to calculate crystallite size (D) from XRD data. Scanning electron microscopy (FE-SEM QUANTA 200 FEG from FEI Netherlands with accelerating voltage 0.3–30 kV) was used to analyze the surface morphology and microstructures of the powdered samples. The compositional purity and stoichiometry of various cations were checked by energy-dispersive X-ray spectroscopy (EDX) using INCA attachment with the SEM instrument. Transmission electron microscopy (TEM) was used to measure grain size of the samples. The M-H curves were obtained at 300 K employing vibrating sample magnetometer (VSM) having magnetic field of 15 kOe.

Results and discussion

Figure 1 gives the XRD pattern for $\text{NiFe}_{2-x}\text{La}_x\text{O}_4$ ferrites at 300 K and Rietveld profile fitting for the data. All the diffraction maxima were well indexed and matched well with cubic NiFe_2O_4 (JCPDS Card No. 44–1485). The appearance of the major lattice planes (220), (311), (222), (422), (511), (400), and (440) evidences the formation of cubic spinel structures with space group $Fd\bar{3}m$ (227). Very small peaks of Fe_2O_3 ($a = 5.0351(2)\text{\AA}$, $c = 13.7545(9)\text{\AA}$; space group $R\bar{3}c$) and LaFeO_3 ($a = 5.5583(4)\text{\AA}$, $b = 5.5586(3)\text{\AA}$, $c = 7.8516(3)\text{\AA}$; space group $Pbnm$) characteristic of secondary phases were also noticed, which intensity increases with increase in La content indicating slight solid solubility of La^{3+} . Using the following relation, the weight% of orthoferrite (LaFeO_3) has been calculated

$$\begin{aligned} &\text{Weight\% of orthoferrite} \\ &= \left(\frac{I_{\text{orthoferrite}}}{I_{\text{orthoferrite}} + I_{\text{spinel ferrite}} + I_{\text{Fe}_2\text{O}_3}} \right) \times 100 \end{aligned}$$

and the calculated values of weight% of orthoferrite, Fe_2O_3 , and spinel phases are tabulated in Table 1. From the table, it can be noticed that weight% of spinel phase decreased with La exchange. Hence, it can be inferred that even a little mass of La^{3+} in NiFe_2O_4 can influence the phase composition and also the size of the spinel matrix, that is, because of the formation of orthoferrite (LaFeO_3) phase.

For complete structural information of the synthesized phases, Rietveld refinement was made on the XRD data using the *GSAS/EXPGUI* program [35] by using essential structural data from the literature. The standard of refinement was confirmed through various parameters like R_{wp} , R_p , and χ^2

Fig. 1 Rietveld profile fitting for the XRD patterns of $\text{NiFe}_{2-x}\text{La}_x\text{O}_4$

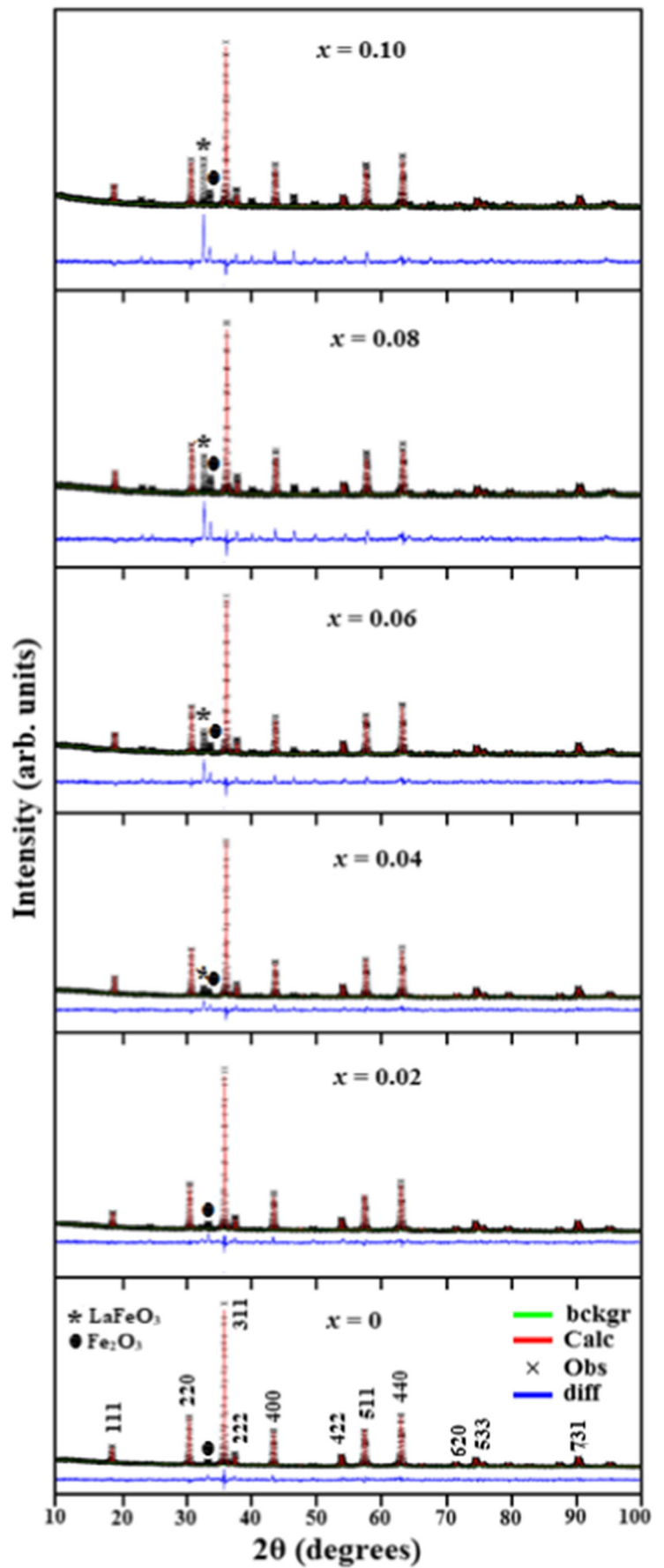


Table 1 Phase analysis of NiFe_{2-x}La_xO₄

<i>x</i>	0.0	0.02	0.04	0.06	0.08	0.10
Weight% of spinel phase	97.3	92.9	91.4	82.1	75.5	72.6
Weight% of orthoferrite	0	2.9	4.2	12.5	17.3	20.1
Weight% of Fe ₂ O ₃	2.7	4.2	4.4	5.4	7.2	7.3

collected from refinement. A relatively good fit between the observed and calculated diffraction patterns (Fig. 1) is observed. The refined structural parameters for the samples are summed in Table 2. It can be observed from Table 2 that the lattice parameter *a* rises initially and then start decreasing with further La doping. The rise in lattice parameter *a* with $x \leq 0.04$ might be due to larger ionic radius of lanthanum (1.061 Å) than iron (0.645 Å) resulting in the increase of unit cell volume, which confirms the entry of La into the lattice site. The decrease in *a* with $0.04 < x \leq 0.1$ might be due to lower solubility of La³⁺ in the spinel lattice. The expendable La³⁺ ions occupy the grain boundaries forming LaFeO₃ phase whose concentration rises with La doping which is established by XRD results, thus restraining the grain growth and applying pressure on the grains affecting the lattice value *a* to decrease [32, 36, 37].

The crystallite sizes were calculated by Scherrer equation [38] using (311) peak of highest intensity

$$D = \frac{K\lambda}{\beta \cos\theta}$$

where *K* is the shape factor (= 0.90), λ is the X-ray wavelength, θ corresponds to the peak position, and β is full width at half maximum of (311) peak in radians and their values are listed in Table 2. It is recognized that La doping has nearly no impact on the crystallite size of Ni ferrites.

To check the compositional purity and stoichiometry of constitutive elements, EDX measurements were carried on synthesized samples. Typical EDX spectra for $x = 0.0$ and

0.02 samples are given in Fig. 2. The EDX results confirmed the presence of Ni, Fe, La, and O and did not reveal the presence of any foreign element in the phases. The mass percentages obtained from EDX were found near to the nominal compositions as presented in Table 3. Thus, the glycine-nitrate combustion technique used in this work is a suitable method for sample synthesis with good stoichiometry.

The microstructures and grain sizes of the calcined ferrite powders were determined by SEM method considering the average of a large number of grains. FE-SEM profile of $x = 0$ and 0.02 phases are displayed in Fig. 3. Both the samples display the formation of spongy and fragile nickel ferrite powders with empty spaces and pores in the samples. It is due to the liberation of a considerable mass of gases during the combustion process due to the decomposition of both glycine and metal nitrates. This clearly shows that the results of SEM are dependent on the type of raw materials used, as well as on the synthetic methods. It is further revealed by SEM profile that the aggregated particles lie in the nanometric range. The materials show some tendency of aggregation because of their magnetic properties.

In order to have a detailed information regarding particle dimensions and morphology, TEM images of the prepared ferrites for $x = 0.0$ and 0.02 compositions were obtained (Fig. 4). The TEM micrographs of the synthesized samples revealed the spherical shape of nanoparticles with a small particle size distribution. The line intercept method was followed to determine the average grain size and found to be 56 nm and 58 nm, respectively, for $x = 0.0$ and 0.02 compositions, which are in good agreement with the crystallite sizes obtained from XRD.

The magnetization behavior of ferrite particles is attributed to various characteristics like synthetic method, cation distribution among octahedral and tetrahedral sites, crystallite size, and spin-orbital coupling strength [39, 40]. Figure 5 presents the typical graphs for the hysteresis loops of NiFe_{2-x}La_xO₄ samples at room temperature. The magnetic properties like saturation magnetization (*M_s*), remanent magnetization (*M_r*),

Table 2 Structural parameters obtained from the Rietveld refinement of X-ray diffraction pattern for NiFe_{2-x}La_xO₄ samples calcined at 800°C temperature

Sample	$x = 0.0$	$x = 0.02$	$x = 0.04$	$x = 0.06$	$x = 0.08$	$x = 0.10$
<i>a</i> (Å)	8.3357 (1)	8.3362 (1)	8.3379 (1)	8.3346 (1)	8.3340 (2)	8.3339 (2)
<i>u</i>	0.2546(3)	0.2537 (3)	0.2547 (3)	0.2551 (4)	0.2552 (5)	0.2554 (6)
<i>D</i> (nm)	61.4	61.6	62.3	62.4	62.6	62.9
<i>R_{wp}</i> (%)	6.78	7.73	7.81	9.87	11.70	12.38
<i>R_p</i> (%)	5.28	5.80	5.68	6.77	7.65	7.86
χ^2	1.052	1.310	1.344	1.902	2.593	2.913

The atomic sites are Ni/Fe 8a [0.125, 0.125, 0.125], Fe/La 16d[0.5, 0.5, 0.5] and O 32e in the space group *Fd3̄m*

Table 3 EDX results of $\text{NiFe}_{2-x}\text{La}_x\text{O}_4$ samples

Samples	$x = 0.0$		$x = 0.02$	
	Element	Experimental mass%	Theoretical mass%	Experimental mass%
Ni	24.71	25.04	24.26	24.86
La	-	-	1.32	1.18
Fe	46.91	47.65	46.26	46.85

and coercivity (H_c) were estimated from the hysteresis curve, and their values are summarized in Table 4. It can be seen that M_s reduces from 54.934 emu/g for $x = 0.0$ to 26.696 emu/g for $x = 0.1$ sample by the replacement of Fe^{3+} magnetic ions by La^{3+} ions which could be due to the effect of cation distribution among tetrahedral and octahedral sites. In the normal structural model for ferrites possessing collinear ferrimagnetic structure, the magnetization of tetrahedral (A) site is antiparallel to that of octahedral (B) site. Due to larger ionic radius of La^{3+} ions than Ni^{2+} and Fe^{3+} ions, La^{3+} ions favor to hold the octahedral sublattice (B). Moreover, La^{3+} is a diamagnetic ion; the major contribution to the magnetic properties of $\text{NiFe}_{2-x}\text{La}_x\text{O}_4$ ferrites will appear from Fe^{3+} ions ($5\mu_B$) on the B sublattice. Thus, exchange of Fe^{3+} on B sublattice by La^{3+} lowers the super exchange interactions, overall magnetic moment ($\mu = \mu_B - \mu_A$) and hence lessen the saturation magnetization. In addition, spin canting generally produced by

rare earth ions transforms collinear ferromagnetic order into non-collinear ordering thereby disrupting ferrimagnetic order, thus leading to a decrease in M_s [41]. Furthermore, the decrease in saturation magnetization could also be due to existence of antiferromagnetic LaFeO_3 component which becomes dominant with La doping [35, 42].

The magnetic moment per formula unit in Bohr magneton (n_B) for La^{3+} doped nickel ferrites, as given in Table 4, is measured using the relationship given below [43]:

$$n_B = \frac{M_W \times M_s}{5585}$$

where M_W is the molecular weight of a specific ferrite structure and M_s is the saturation magnetization (emu/g). The reduction in n_B from $2.243\mu_B$ for $x = 0.0$ to $0.842\mu_B$ for $x = 0.10$ with the rise of La^{3+} replacement in Ni ferrites is seen, which is completely compatible

Fig. 2 EDX spectrum of $\text{NiFe}_{2-x}\text{La}_x\text{O}_4$ for $x = 0$ and 0.02

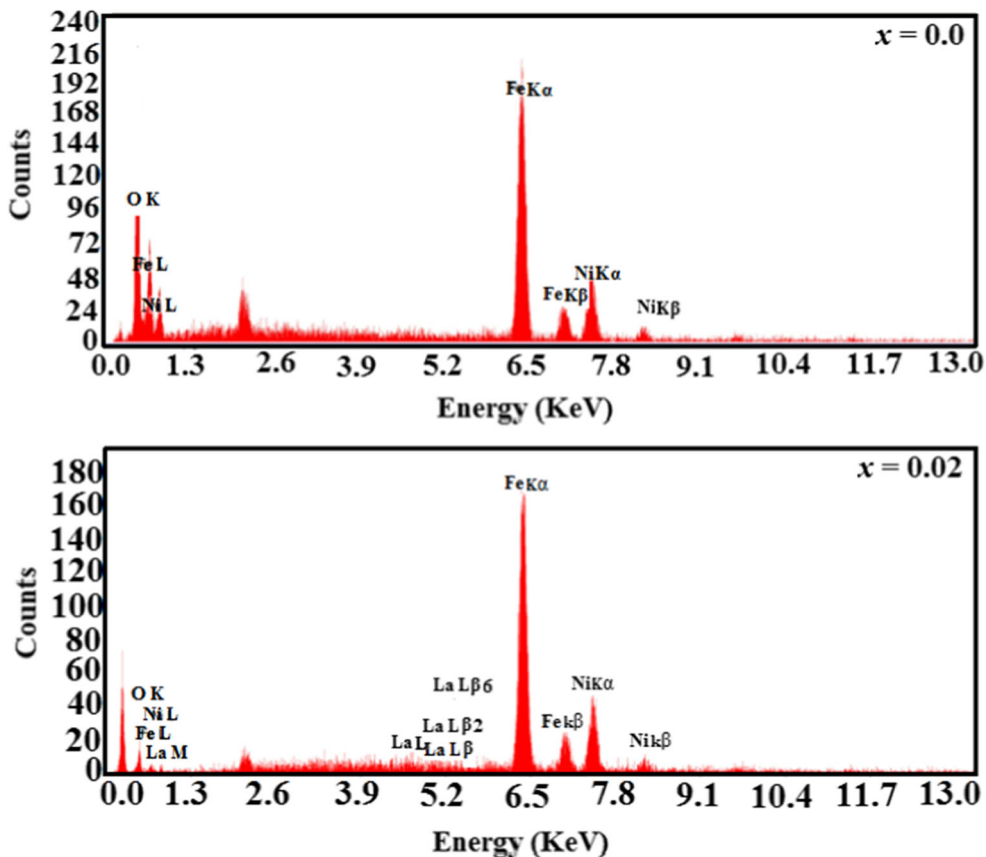
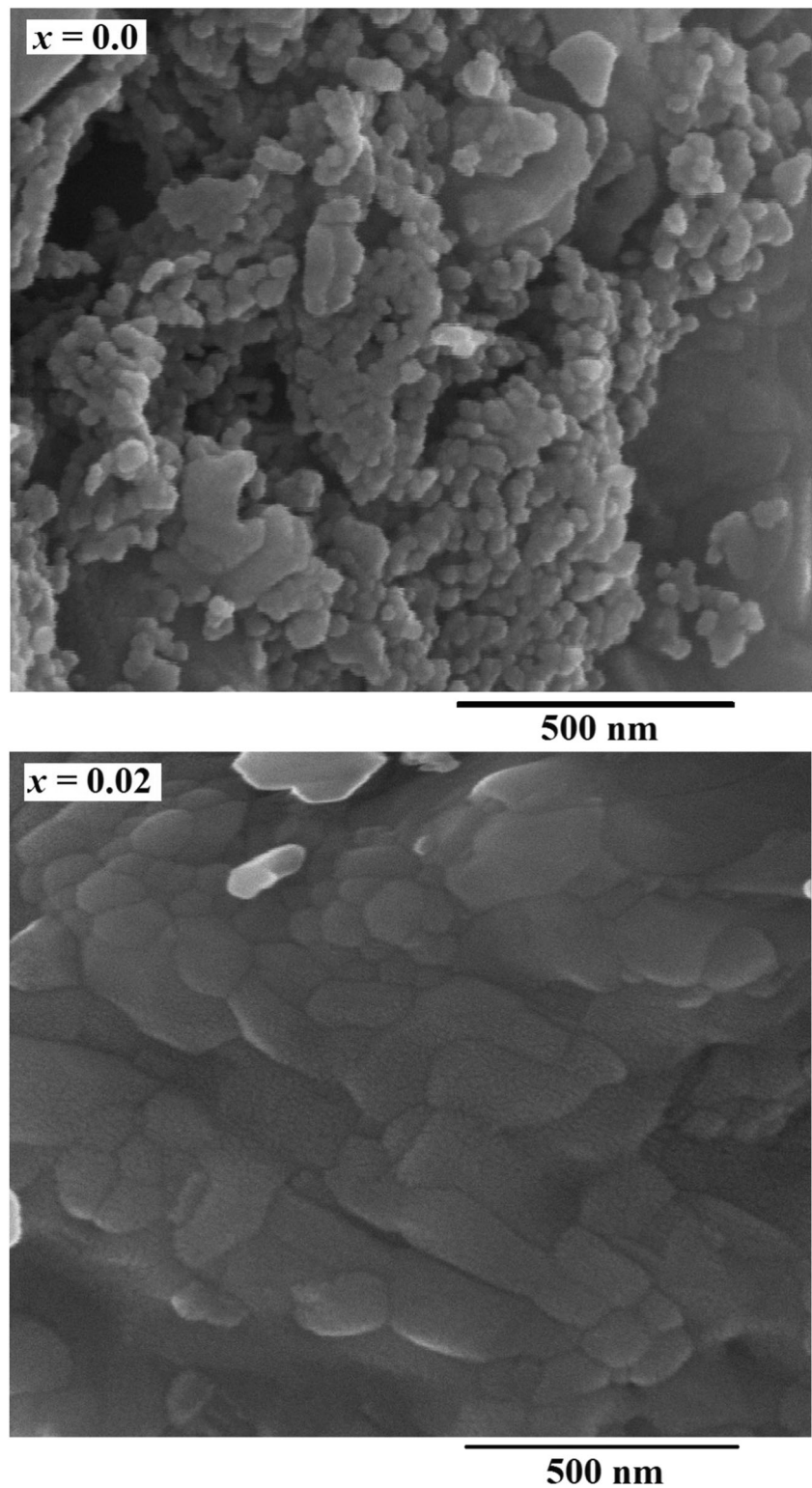


Fig. 3 FE-SEM micrographs of polycrystalline powders of $\text{NiFe}_{2-x}\text{La}_x\text{O}_4$ for $x = 0$ and 0.02



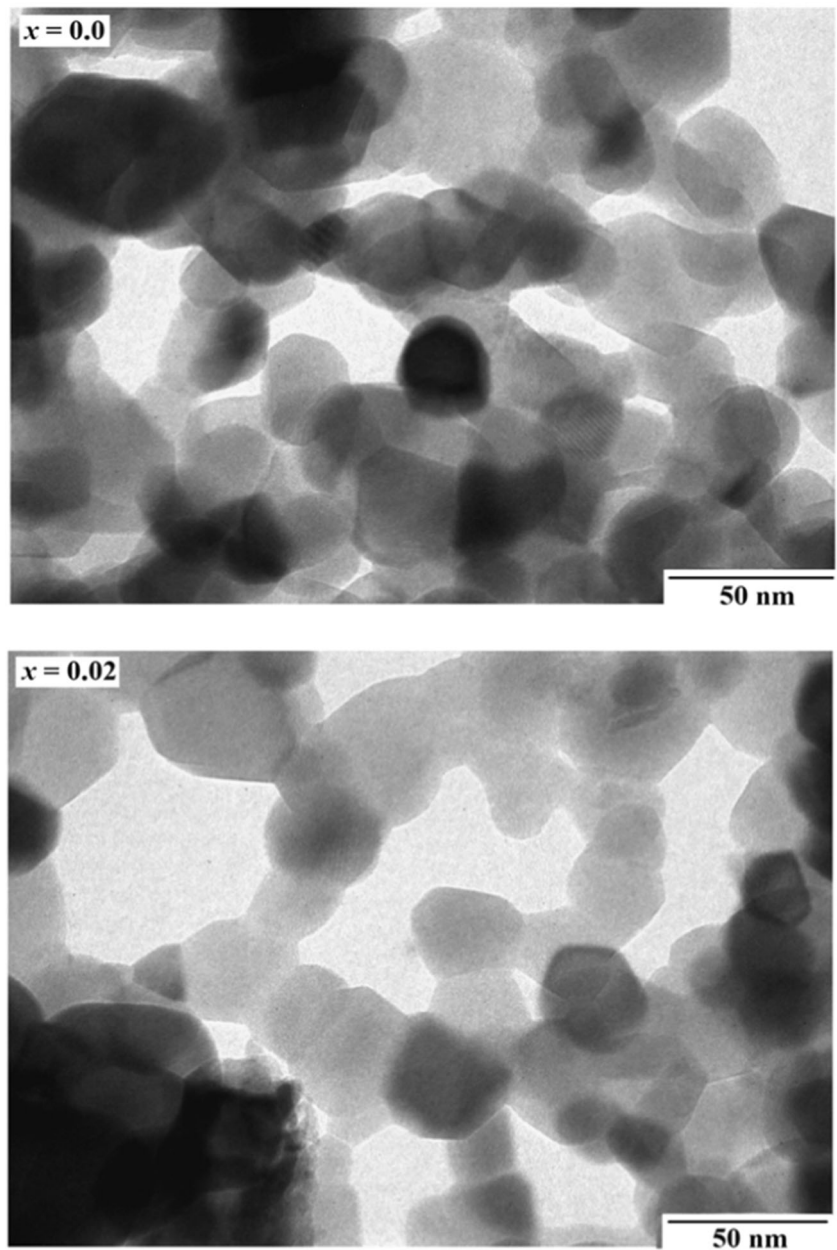
with the behavior of M_s . Same consequences had been noticed for Gd doped Co ferrites [40].

Since La^{3+} ions primarily reside the octahedral sites due to their large size, the proposed cation distribution of $\text{NiFe}_{2-x}\text{La}_x\text{O}_4$ ferrites can thus be written as $[\text{Fe}][\text{NiFe}_{1-x}\text{La}_x]\text{O}_4$

assuming all Ni^{2+} ions occupy octahedral voids. The theoretical magnetic moment, $n_B(\text{th})$, can be calculated by the relation

$$n_B(\text{th}) = \mu(\text{octahedral site}) - \mu(\text{tetrahedral site})$$

Fig. 4 TEM micrograph of $\text{NiFe}_{2-x}\text{La}_x\text{O}_4$ for $x = 0$ and 0.02



and its values are listed in Table 4. These values are found to be slightly larger (except $x = 0.0$) than those obtained from M–

H loops. In order to have good agreement between n_B and $n_B(\text{th})$, the value of $n_B(\text{th})$ should be decreased by changing

Table 4 Magnetic parameters of $\text{NiFe}_{2-x}\text{La}_x\text{O}_4$

x	Coercivity, H_c (G)	Saturation magnetization, M_s (emu/g)	Remanence, M_r (emu/g)	Magnetic moment (from MH loop), n_B (B.M.)	Theoretical magnetic moment, n_B (th) (B.M.)
0.0	158.31	54.934	5.2355	2.243	1.946
0.02	286.98	36.800	11.447	1.445	1.765
0.04	269.61	36.671	11.578	1.426	1.645
0.06	278.28	31.169	9.8380	1.097	1.396
0.08	274.26	26.890	8.0327	0.876	1.208
0.10	282.51	26.696	8.4436	0.842	1.089

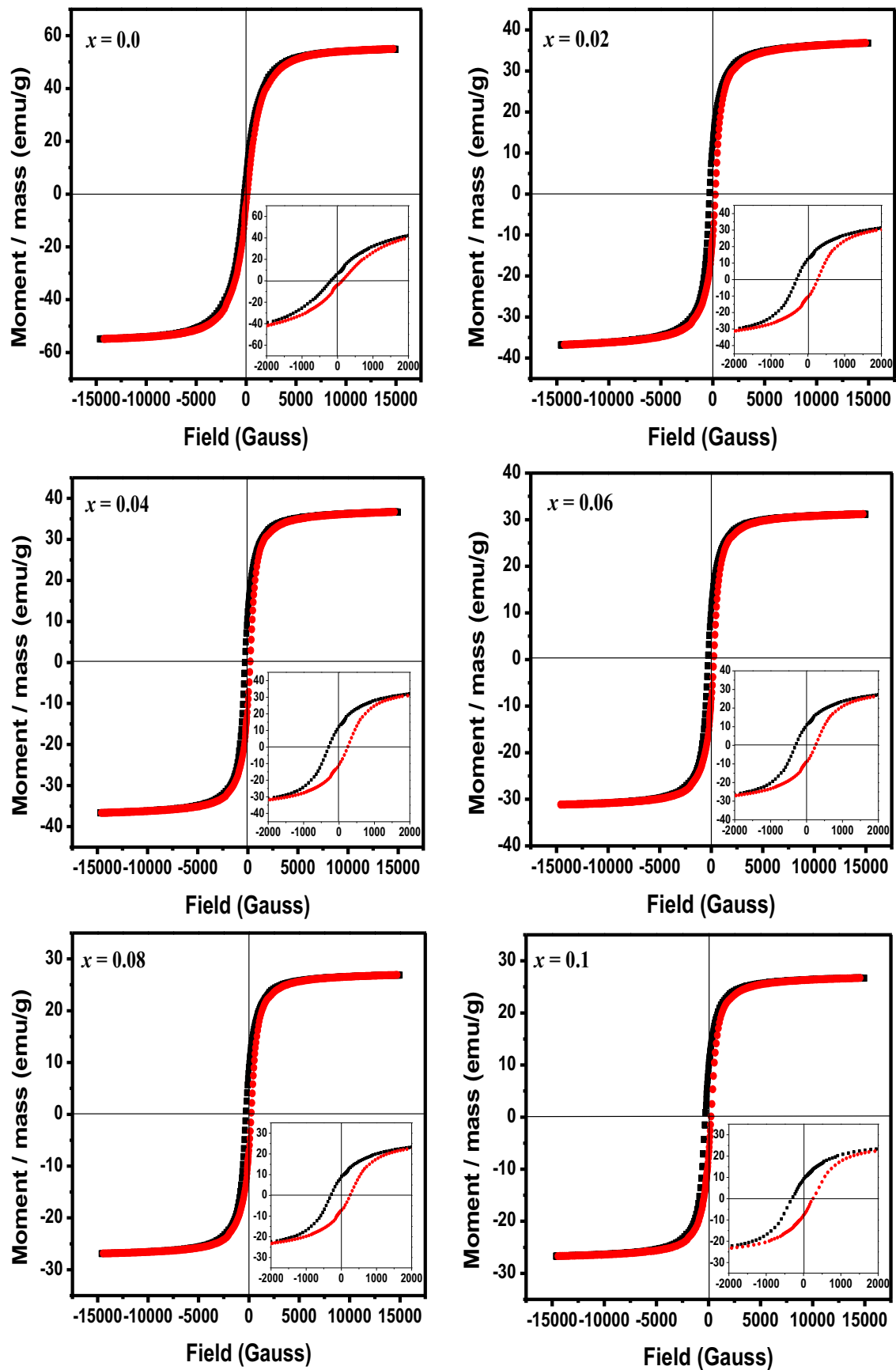


Fig. 5 Variation of magnetization with applied field for $\text{NiFe}_{2-x}\text{La}_x\text{O}_4$

the cation distribution. Moreover, the $n_B(\text{th})$ values cannot be further decreased as Ni^{2+} ions having lower magnetic moment than Fe^{3+} ions are already assumed to be present at octahedral sites, thus confirming the cation distribution to be $[\text{Fe}][\text{NiFe}_{1-x}\text{La}_x]\text{O}_4$. The smaller value of $n_B(\text{th})$ than that of n_B obtained from M–H loop in case of $x = 0.0$ indicates the presence of some Ni^{2+} ions at tetrahedral sites, and its cation distribution can therefore be written as $[\text{Ni}_{0.05}\text{Fe}_{0.95}][\text{Ni}_{0.95}\text{Fe}_{1.05}]\text{O}_4$. Further, as can be seen from Table 4 that the value of coercivity force is not significant variation with the increasing La doping. It may be correlated to the coercivity which is affected by various factors, such as crystallinity, microstrain, magnetic particle morphology and size distribution, anisotropy, and magnetic domain size [44, 45].

Conclusions

Lanthanum substituted cobalt ferrites $\text{NiFe}_{2-x}\text{La}_x\text{O}_4$ ($0.0 \leq x \leq 0.10$) have been synthesized via combustion method using glycine as a fuel. All the ferrites crystallize in space group with cubic symmetry. The lattice parameter a first increases for $x = 0.0$ to $x = 0.04$ and then starts decreasing. The particle sizes estimated from TEM are in good agreement with the crystallite size calculated from XRD using Scherrer's formula. Magnetic measurements showed that all the samples possess ferromagnetic behavior. Replacement of Fe^{3+} on B sublattice by diamagnetic La^{3+} decreases the superexchange interactions and consequently lowers the saturation magnetization.

Declarations

Conflict of interest The authors declare no competing interests.

References

- Burianova, S., Vejpravova, J.P., Holec, P., Plocek, J., Niznansky, D.: Surface spin effects in La-doped CoFe_2O_4 nanoparticles prepared by microemulsion route. *J. Appl. Phys.* **110**(1–7), 073902 (2011)
- Andersen, H.L., Christensen, M.: In situ powder X-ray diffraction study of magnetic CoFe_2O_4 nanocrystallite synthesis. *Nanoscale*. **7**, 3481–3490 (2015)
- Pöttker, W.E., Ono, R., Cobos, M.A., Hernando, A., Araujo, J.F., Bruno, A.C., Lourenco, S.A., Longo, E., La Porta, F.A.: Influence of order-disorder effects on the magnetic and optical properties of NiFe_2O_4 nanoparticles. *Ceram. Int.* **44**, 17290–17297 (2018)
- Araujo, J.F., Vieira, D.R., Osorio, F., Pöttker, W.E., La Porta, F.A., de la Presa, P., Perez, G., Bruno, A.C.: Versatile Hall magnetometer with variable sensitivity assembly for characterization of the magnetic properties of nanoparticles. *J. Magn. Magn. Mater.* **13**(1–8), 165431 (2019)
- Shirsath, S.E., Jadhav, S.S., Toksha, B.G., Patange, S.M., Jadhav, K.M.: Influence of Ce^{4+} ions on the structural and magnetic properties of NiFe_2O_4 . *J. Appl. Phys.* **110**(1–8), 013914 (2011)
- Goldman, A.: *Modern Ferrite Technology*. Marcel Dekker, New York (1993)
- Ozgun, U., Alivov, Y., Morkoc, Y.: Microwave ferrites, part 1: fundamental properties. *J. Mater. Sci. Mater. Electron.* **20**, 799–834 (2009)
- Slimani, Y., Almessiere, M.A., Güner, S., Kurtan, U., Shirsath, S.E., Baykal, A., Ercan, I.: Magnetic and microstructural features of Dy^{3+} substituted NiFe_2O_4 nanoparticles derived by sol–gel approach. *J. Sol-Gel Sci. Technol.* **95**, 202–210 (2020)
- Albetran, H., Slimani, Y., Almessiere, M.A., Alahmari, F., Shirsath, S.E., Akhtar, S., Low, I.M., Baykal, A., Ercan, I.: Synthesis, characterization and magnetic investigation of Er-substituted electrospun NiFe_2O_4 nanofibers. *Phys. Scr.* **95**, 075801 (2020)
- Bharathi, K.K., Balamurugan, K., Santhosh, P., Pattabiraman, M., Markandeyulu, G.: Magnetocapacitance in Dy-doped Ni ferrite. *Phys. Rev. B.* **77**, 172401 (2008)
- Schloemann, E.: Advances in ferrite microwave materials and devices. *J. Magn. Magn. Mater.* **209**, 15–20 (2000)
- Ateia, E., Ahmed, M.A., El-Aziz, A.K.: Effect of rare earth radius and concentration on the structural and transport properties of doped Mn–Zn ferrite. *J. Magn. Magn. Mater.* **311**, 545–554 (2007)
- Ahmed, M.A., Okasha, N.N., El-Sayed, M.M.: Enhancement of the physical properties of rare-earth-substituted Mn–Zn ferrites prepared by flash method. *Ceram. Int.* **33**, 49–58 (2007)
- Kinemuchi, Y., Ishizaka, K., Suematsu, H., Jiang, W., Yatsui, K.: Magnetic properties of nanosize NiFe_2O_4 particles synthesized by pulsed wire discharge. *Thin Solid Films.* **407**, 109–113 (2002)
- Ognjanovic, S.M., Tokic, I., Cvejic, Z., Rakic, S., Srdic, V.V.: Structural and dielectric properties of yttrium substituted nickel ferrites. *Mater. Res. Bull.* **49**, 259–264 (2014)
- Auwal, I.A., Ünal, B., Güngüneş, H., Shirsath, S.E., Baykal, A.: Dielectric properties, cationic distribution calculation and hyperfine interactions of La^{3+} and Bi^{3+} doped strontium hexaferrites. *Ceram. Int.* **42**, 9100–9115 (2016)
- Chaudhari, V., Kadam, R.H., Mane, M.L., Shirsath, S.E., Kadam, A.B., Mane, D.R.: Effect of La^{3+} impurity on magnetic and electrical properties of Co–Cu–Cr–Fe nanoparticles. *J. Nanosci. Nanotechnol.* **15**, 4268–4275 (2015)
- Deraz, N.M., Hessien, M.M.: Structural and magnetic properties of pure and doped nanocrystalline cadmium ferrite. *J. Alloys Compd.* **475**, 832–839 (2009)
- Browne, M.P., Vasconcelos, J.M., Coelho, J., O'Brien, M., Rovetta, A.A., McCarthy, E.K., Nolan, H., Duesberg, G.S., Nicolosi, V., Colavita, P.E., Lyons, M.E.: Improving the performance of porous nickel foam for water oxidation using hydrothermally prepared Ni and Fe metal oxides. *Sustain. Energy Fuels.* **1**, 207–216 (2017)
- Kenfack, F., Langbein, H.: Spinel ferrites of the quaternary system Cu–Ni–Fe–O: Synthesis and characterization. *J. Mater. Sci.* **41**, 3683–3693 (2006)
- Berger, R., Bissey, J.C., Kliava, J., Daubric, H., Estournès, C.: Temperature dependence of superparamagnetic resonance of iron oxide nanoparticles. *J. Magn. Magn. Mater.* **234**, 535–544 (2001)
- Ataie, A., Piramoon, M.R., Harris, I.R., Ponton, C.B.: Effect of hydrothermal synthesis environment on the particle morphology, chemistry and magnetic properties of barium hexaferrite. *J. Mater. Sci.* **30**, 5600–5606 (1995)
- Davies, K.J., Wells, S., Upadhyay, R.V., Charles, S.W., O'Grady, K., Hilo, M.E., Meaz, T., Mørup, S.: The observation of multi-axial anisotropy in ultrafine cobalt ferrite particles used in magnetic fluids. *J. Magn. Magn. Mater.* **149**, 14–18 (1995)
- Chen, J.P., Sorensen, C.M., Klabunde, K.J., Hadjipanayis, G.C., Devlin, E., Kostikas, A.: Size-dependent magnetic properties of

- MnFe₂O₄ fine particles synthesized by coprecipitation. *Phys. Rev. B.* **54**, 9288 (1996)
25. Sisk, M., Kilbride, I., Barker, A.J.: Production of manganese zinc ferrites via the hydrothermal decomposition of metal (III) acetates and citrates. *J. Mater. Sci. Lett.* **14**, 153–154 (1995)
 26. Poddar, P., Srikanth, H., Morrison, S.A., Carpenter, E.E.: Interparticle interactions and magnetism in manganese–zinc ferrite nanoparticles. *J. Magn. Magn. Mater.* **288**, 443–451 (2005)
 27. Alarif, A., Deraz, N.M., Shaban, S.: Structural, morphological and magnetic properties of NiFe₂O₄ nano-particles. *J. Alloys Compd.* **486**, 501–506 (2009)
 28. Liu, T., Xu, Y.: Synthesis of nanocrystalline LaFeO₃ powders via glucose sol–gel route. *Mater. Chem. Phys.* **129**, 1047–1050 (2011)
 29. Shen, H., Cheng, G., Wu, A., Xu, J., Zhao, J.: Combustion synthesis and characterization of nano-crystalline LaFeO₃ powder. *Phys. Status Solidi A.* **206**, 1420–1424 (2009)
 30. Qi, X., Zhou, J., Yue, Z., Gui, Z., Li, L.: Auto-combustion synthesis of nanocrystalline LaFeO₃. *Mater. Chem. Phys.* **78**, 25–29 (2002)
 31. Al Angari, Y.M.: Magnetic properties of La-substituted NiFe₂O₄ via egg-white precursor route. *J. Magn. Magn. Mater.* **323**, 1835–1839 (2011)
 32. Lin, Q., Yuan, G., He, Y., Wang, L., Dong, J., Yu, Y.: The influence of La-substituted Cu_{0.5}Co_{0.5}Fe₂O₄ nanoparticles on its structural and magnetic properties. *Mater. Des.* **78**, 80–84 (2015)
 33. Jain, S.R., Adiga, K.C., Verneker, V.P.: A new approach to thermochemical calculations of condensed fuel-oxidizer mixtures. *Combust. Flame.* **40**, 71–79 (1981)
 34. Singh, S., Singh, D.: Synthesis of LaFeO₃ nanopowders by glycine–nitrate process without using any solvent: effect of temperature. *Monatsh. Chem.* **148**, 879–886 (2017)
 35. Larson, A.C., Dreele, R.B.V.: General Structure Analysis System (GSAS), Los Alamos National Laboratory Report LAUR. 86–748 (2004)
 36. Verma, S., Chand, J., Singh, M.: Effect of In³⁺ ions doping on the structural and magnetic properties of Mg_{0.2}Mn_{0.5}Ni_{0.3}In_xFe_{2–x}O₄ spinel ferrites. *J. Magn. Magn. Mater.* **324**, 3252–3260 (2012)
 37. Heiba, Z.K., Mohamed, M.B., Arda, L., Dogan, N.: Cation distribution correlated with magnetic properties of nanocrystalline gadolinium substituted nickel ferrite. *J. Magn. Magn. Mater.* **391**, 195–202 (2015)
 38. Klug, H.P., Alexander, L.E.: X-ray diffraction procedures; for polycrystalline and amorphous materials. John Wiley and Sons Inc, Canada (1954)
 39. Franco Jr., A., Silva, M.S.: High temperature magnetic properties of magnesium ferrite nanoparticles. *J. Appl. Phys.* **109**, 07B505 (2011)
 40. Kahn, M.L., Zhang, Z.J.: Synthesis and magnetic properties of CoFe₂O₄ spinel ferrite nanoparticles doped with lanthanide ions. *Appl. Phys. Lett.* **78**, 3651–3653 (2001)
 41. Wang, Y., Xu, F., Li, L., Liu, H., Qiu, H., Jiang, J.: Magnetic properties of La-substituted Ni–Zn–Cr ferrites via rheological phase synthesis. *Mater. Chem. Phys.* **112**, 769–773 (2008)
 42. Mahadevan, P., Shanthi, N., Sarma, D.D.: Electronic structure of LaCrO₃, LaMnO₃ and LaFeO₃ from *ab initio* spin-polarized calculations. *J. Phys. Condens. Matter.* **9**, 3129–3138 (1997)
 43. Hankare, P.P., Jadhav, S.D., Sankpal, U.B., Chavan, S.S., Waghmare, K.J., Chougule, B.K.: Synthesis, characterization and effect of sintering temperature on magnetic properties of Mg–Ni ferrite prepared by co-precipitation method. *J. Alloys Compd.* **475**, 926–929 (2009)
 44. Hashim, M., Shirsath, S.E.A., Meena, S.S., Kotnala, R.K., Kumar, S., Bhatt, P., Jotania, R.B., Kumar, R.: Study of structural and magnetic properties of (Co–Cu) Fe₂O₄/PANI composites. *Mater. Chem. Phys.* **141**, 406–415 (2013)
 45. Kavanlou, M., Hashemi, B.: Effect of B₂O₃ on the densification and magnetic properties of Li–Zn ferrite. *Mater. Des.* **32**, 4257–4261 (2011)

Publisher's note Springer Nature remains neutral with regard to jurisdictional claims in published maps and institutional affiliations.